Article

# ZnS Nanomaterial Characterization by MALDI-TOF Mass Spectrometry

Gregory A. Khitrov, and Geoffrey F. Strouse

*J. Am. Chem. Soc.*, **2003**, 125 (34), 10465-10469• DOI: 10.1021/ja035508r • Publication Date (Web): 01 August 2003



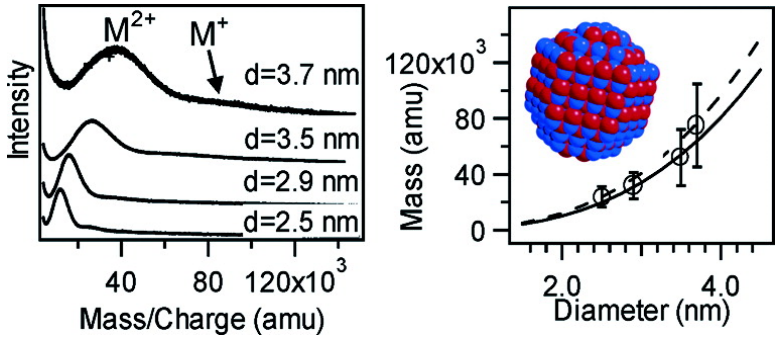


## More About This Article

Additional resources and features associated with this article are available within the HTML version:

- Supporting Information
- Links to the 5 articles that cite this article, as of the time of this article download
- Access to high resolution figures
- Links to articles and content related to this article
- Copyright permission to reproduce figures and/or text from this article

View the Full Text HTML

J|A|C|S
ARTICLES
Published on Web 08/01/2003

# ZnS Nanomaterial Characterization by MALDI-TOF Mass Spectrometry

Gregory A. Khitrov and Geoffrey F. Strouse*

*Contribution from the Department of Chemistry and Biochemistry, University of California, Santa Barbara, California 93106*

Received April 7, 2003; E-mail: strouse@chem.ucsb.edu

***Abstract:*** We present a methodology for mass and size dispersity analysis by MALDI-TOF mass spectrometry of lyothermally grown 2.5−3.7 nm ZnS nanocrystals having a Zn blende crystal structure. These results correlate with information obtained by TEM and absorption spectroscopy. The use of MS methods to probe size and size dispersity provides a convenient method to rapidly analyze II−VI materials at the nanoscale. We believe these results represent the first mass spectrometric analysis of size and size dispersities on II−VI nanocrystals.

Due to the size-dependent nature of nanoscale materials, the size, shape, and dispersity must be accurately known for applications in device technology.[1] These materials, when grown lyothermally, typically exhibit a 5−10% size dispersity as spherical, crystalline fragments of a bulk lattice stabilized by an organic passivating layer. Traditionally, optical spectroscopy coupled to either transmission electron microscopy (TEM) or powder XRD (pXRD) analysis is typically employed as a measure of shape, size, and size distributions for nanocrystal samples. Calculation of size from pXRD data by fitting to the Scherer equation has inherent inaccuracies, as the pXRD peak width is also affected by the shape and size distribution of the nanocrystals.[2] Measuring the shape, size, and size distribution from TEM images involves another set of uncertainties, as the measurement of size and size distribution is very subjective and the resolution is dependent on the contrast, which can be low for nanomaterials of lighter elements. Attempts to utilize high-performance liquid chromatography (HPLC) have shown promise for determination of size and size distribution for several metal and semiconductor nanomaterials, but the technique suffers from the strong dependence of the sample retention time on the interaction of the capping ligands with the separation column.[2] An alternative analytical technique, which is often used for compositional analysis, is mass spectrometry. Mass spectrometric (MS) methods can provide a very accurate method for measuring mass and, therefore, sizes and size distributions of nanomaterial samples.

Mass spectrometric methods have been demonstrated to provide valuable insight into the structure of a wide range of materials such as biological,[3,4] polymer,[5] and nanoscale materials.[9−10] Thiol-passivated Au nanocrystals, prepared in solution, were analyzed in the 1.5−3.5 nm size range (10−1000 Au atoms) by laser desorption ionization (LDI) mass spectrometry, resulting in a very accurate analysis of the shape, size, and passivation of these nanomaterials.[10] In addition,

(1) (a) Eychmuller, A. *J. Phys. Chem.* **2000**, *104*, 6514. (b) Brus, L. *J. Phys. Chem.* **1986**, *90*, 2555. (c) Brus, L. E. *Appl. Phys. A* **1991**, *53*, 465. (d) Nirmal, M.; Brus, L. *Acc. Chem. Res.* **1999**, *32*, 407. (e) Brus, L. E.; Trautman, J. K. *Philos. Trans. R. Soc. London, Sect. A* **1995**, *353*, 313. (f) Wang, Y.; Herron, N. *J. Phys. Chem.* **1991**, *95*, 525. (g) Banyai, L.; Koch, S. W. *Semiconductor Quantum Dots*; World Scientific: Singapore, 1993. (h) Weller, H. *Angew. Chem., Int. Ed. Engl.* **1993**, *32*, 41. (i) Weller, H. *Adv. Mater.* **1993**, *5*, 88. (j) Alivisatos, A. P. *J. Phys. Chem.* **1996**, *100*, 13226. (k) Waggon, U. *Optical Properties of Semiconductor Quantum Dots*; Springer-Verlag: Berlin, 1997. (l) Gaponenko, S. V. *Optical Properties of Semiconductor Nanocrystals*; Cambridge University Press: Cambridge, 1998. (m) Green, M.; O'Brien, P. *Chem. Commun.* **1999**, 2235. (n) Henglein, A. *Top. Curr. Chem.* **1988**, *143*, 113. (o) Henglein, A. *Chem. Rev.* **1989**, *89*, 1861. (p) Empedocles, S.; Bawendi, M. *Acc. Chem. Res.* **1999**, *32*, 389. (q) Murphy, C. J.; Coffer, J. L. *Appl. Spectrosc.* **2002**, *56*, 16A−27A.

(2) (a) Wilcoxon, J. P.; Martin, J. E.; Provencio, P. *Langmuir* **2000**, *16*, 9912−9920. (b) Wilcoxon, J. P.; Martin, J. E.; Provencio, P. *J. Chem. Phys.* **2001**, *115*, 998−1008. (c) Wilcoxon, J. P.; Craft, S. A. *Nanostruct. Mater.* **1997**, *9*, 85−88.

(3) (a) Lay, J. O. *Mass Spectrom. Rev.* **2001**, *20*, 172−194. (b) Fuerstenau, S. D.; Benner, W. H.; Thomas, J. J.; Brugidou, C.; Bothner, B.; Siuzdak, G.; *Angew. Chem., Int. Ed.* **2001**, *40*, 542−544. (c) Maleknia, S. D.; Downard, K. *Mass Spectrom. Rev.* **2001**, *20*, 388−401. (d) Veenstra, T. D. *Biophys. Chem.* **1999**, *79*, 63−79.

(4) (a) Beck, J. L.; Colgrave, M. L.; Ralph, S. R.; Sheil, M. M. *Mass Spectrom. Rev.* **2001**, *20*, 61. (b) Koomen, J. M.; Russel, W. K.; Tichy, S. E.; Russel, D. H. *J. Mass Spectrom.* **2002**, *37*, 357−371.

(5) (a) Belu, A. M.; DeSimone, J. M.; Linton, R. W.; Lange, G. W.; Friedman, R. M. *J. Am. Soc. Mass Spectrom.* **1996**, *7*, 11−24. (b) Scrivens, J. H.; Jackson, A. T. *Int. J. Mass Spectrom.* **2000**, *200*, 261−276. (c) Nielen, M. W. F. *Mass Spectrom. Rev.* **1999**, *18*, 309−344. (c) Schwartz, B. L.; Rockwood, A. L.; Smith, R. D.; Tomalia, D. A.; Spindler, R. *Rapid Commun. Mass. Spectrom.* **1995**, *9*, 1552−55. (d) Kriesel, J. W.; Konig, S.; Freitas, M. A.; Marshall, A. G.; Leary, J. A.; Tilley, T. D. *J. Am. Chem. Soc.* **1998**, *120*, 12207−15. (e) Cai, Y.; Peng, W.-P.; Chang, H.-C. *Anal. Chem.* **2003**, *75*, 1805−1811.

(6) Serna, R.; Dreyfus, R. W.; Solis, J.; Afonso, C. N.; Allwood, D. A.; Dyer, P. E.; Petford-Long, A. K. *Appl. Surf. Sci.* **1998**, *127−129*, 383−387.

(7) (a) Fasce, D. P.; Williams, R. J. J.; Erra-Balsells, R.; Ishikawa, Y.; Nonami, H. *Macromolecules* **2001**, *34*, 3534−3539. (b) Smet, P.; Devreese, B.; Verpoort, F.; Pauwels, T.; Svoboda, I.; Foro, S.; Van Beeumen, J.; Verdonck, L. *Inorg. Chem.* **1998**, *37*, 6583−6586. (c) Dyson, P. J.; Johnson, B. F. G.; McIndoe, J. S.; Langridge-Smith, P. R. R. *Inorg. Chem.* **2000**, *39*, 2430−2431. (d) Ruiz-Molina, D.; Gerbier, P.; Rumberger, E.; Amabilino, D. B.; Guzei, I. A.; Folting, K.; Huffman, J. C.; Rheingold, A.; Christou, G.; Veciana, J.; Hendrickson, D. N. *J. Mater. Chem.* **2002**, *12*, 1152−1161.

(8) (a) Brown, T.; Clipston, N. L.; Simjee, N.; Luftmann, H.; Hungerbuhler, H.; Drewello, T. *Int. J. Mass Spectrom.* **2001**, *210/211*, 249−263. (b) Rogner, I.; Birkett, P.; Campbell, E. E. B. *Int. J. Mass Spectrom. Ion Processes* **1996**, *156*, 103−108.

(9) Martin, T. P. *Phys. Rep.* **1996**, *273*, 199−241.

(10) (a) Whetten, R. L.; Khoury, J. T.; Alvarez, M. A.; Murthy, S.; Vezmar, I.; Wang, Z. L.; Stephens, P. W.; Cleveland, C. L.; Luedtke, W. D.; Landman, U. *Adv. Mater.* **1996**, *8*, 428−433. (b) Arnold, R. J.; Reilly, J. P. *J. Am. Chem. Soc.* **1998**, *120*, 1528−1532.

Martin et al. observed MS data for <2.0 nm ZnS clusters generated in the gas phase, demonstrating that MS techniques are applicable to II−VI materials.[9] These studies suggest that MS methods can be used to investigate the mass, size, and size dispersity of nanomaterials.

Although the mass range needed to analyze organically passivated semiconductor nanomaterials is similar to ranges employed in the earlier applications of mass spectrometry, the isotopic contributions in II−VI materials and the mass distributions of the nanomaterial samples complicate the application of mass spectrometry techniques to these systems. The effect of size distributions on the mass spectral features for a 3.5 nm spherical ZnS particle (cubic Zn blende structure) is easily envisioned. A 3.5 nm *n*-hexadecylamine (HDA)-passivated nanomaterial consists of ∼10 lattice planes (3.12 Å) along the [111] direction or 554 Zn−S units with ∼146 HDA ligands, based on complete coverage of the surface Zn atoms.[11a] Ignoring isotopic contributions, the nanomaterial mass would be 54 000 Da for the unpassivated ZnS core or 89 200 Da for the fully passivated particle. A 10% size distribution of the sample (3.5 ± 0.35 nm) complicates the measurement, resulting in a mass range for *only* the ZnS core between 35 700 and 77 600 Da. These effects would lead to a mass peak for a singly charged species on a linear time-of-flight (TOF) MS instrument having a broad Gaussian peak shape without significant resolution. A MS peak for a ZnS nanocrystal in the 3.7−2.5 nm size range will be further broadened by 0.12−0.30% of the average mass by the isotopic distributions of Zn and S, depending on size. On the other hand, the potentially high sensitivity that is achievable for the analysis of average size and size distributions experimentally by treating the fwhm of the observed Gaussian peak shape could provide a rapid and reliable analytical tool for synthetic sample analysis and quality control, a very important development in nanotechnology.

In this study we present the accurate determination of mass and mass distribution of a series of 2.5−3.7 nm ZnS nanocrystals using MALDI-TOF mass spectrometry. Size and size distributions are extracted from the MS data by modeling the particles as spherical Zn blende crystalline lattices with complete loss of surface passivation. These results correlate with the observed TEM and optical data for the samples. To our knowledge this is the first report of a lyothermally prepared II−VI inorganic nanomaterial analyzed by MALDI-MS.

## Experimental Section

HDA-passivated ZnS nanocrystals in the 2.5−3.7 nm range were prepared using a modification of a single source precursor methodology previously described for CdSe and ZnSe nanomaterials.[12] This methodology has since been expanded to the preparation of CdS and ZnS nanomaterials.[13] Briefly, a $N_2$(g) degassed sample of the molecular cluster $Li_4[Zn_{10}S_4(SPh)_{16}]$ (where $^-$SPh is the thiophenylate group) was added to molten hexadecylamine (160 °C) under $N_2$(g). The temperature of the reaction was slowly increased, and nanocrystal growth was monitored by periodic removal of small aliquots of the reaction mixture and measurement of their UV absorbance. Larger aliquots of the reaction mixture were collected when a desired nanomaterial size was reached.

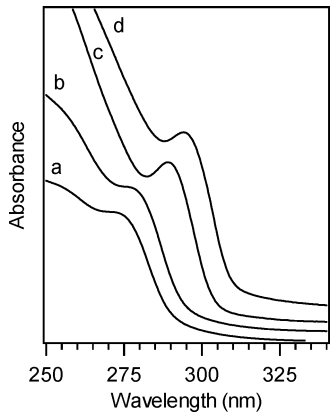


***Figure 1.*** Normalized absorbance spectra in chloroform at 298 ± 2 of (a) 2.5, (b) 2.9, (c) 3.5, and (d) 3.7 nm ZnS-HDA nanocrystals.

The nanomaterials were stored under $N_2$ in the dark in the solidified growth solution at −20 °C. Isolation of the nanomaterials from the growth solution by methyl alcohol-induced precipitation was carried out under airless conditions due to the high propensity for particle oxidation.

Ultraviolet and visible absorption spectra in chloroform were recorded using a Jasco 530 spectrophotometer. Transmission electron microscopy (TEM) was performed on a JEOL 1230 microscope operating at 80 kV in the bright field mode. TEM grids were 400 mesh Cu, coated with a 5 nm layer of holey carbon, purchased from SPI Inc. TEM samples were prepared using standard techniques. Size and size distributions were obtained by manual measurement of nanocrystal images from the digitized micrograph negatives.

MALDI-TOF MS was performed on a Micromass TofSpec 2E instrument using dithranol or anthracene as the matrix. Nanocrystal samples were dispersed in dry chloroform, mixed with chloroform solutions of the matrix, and spotted onto a stainless steel target plate. Desorption and ionization of the samples were achieved by irradiation with a pulsed nitrogen laser (337 nm, 180 $\mu$J/pulse, 4 ns pulses). The fixed energy laser was coupled to a stepped neutral density filter and a continuously variable iris to control the laser energy that reached the sample as a 150 × 250 $\mu$m spot on the target plate. Nanocrystal mass spectra were measured with the laser at 50 and 100% full power. After desorption, a 20 kV potential accelerated the ions into a 1.5 m flight tube (linear TOF mode), which yielded a resolution of 100−200 *m*/*z* in the final mass spectrum. The accuracy of the measured peaks was determined by calibration against the ubiquitous MALDI-MS standards trypsinogen, horse heart myoglobin, cytochrome C, and bovine serum albumin.

## Results and Discussion

The size and size dispersity of the lyothermally prepared, *n*-hexadecylamine-passivated ZnS nanocrystals were estimated from the optical absorbance data for the samples (Figure 1 and Table 1) by comparison to previously published results.[11] A representative TEM (Figure 2) of the 3.7 nm (3.7 ± 0.48 nm) ZnS verifies the size estimates from absorption spectroscopy. Materials below 3.7 nm present difficulty in obtaining an accurate size analysis in the TEM images due to low contrast and a propensity for ablation in the electron beam.

MALDI-TOF mass spectra for the 2.5, 2.9, 3.5, and 3.7 nm diameter ZnS nanocrystals are presented in Figure 3a. The data for each nanocrystal sample exhibit a single high-intensity, Gaussian-shaped peak centered at *m*/*z* values of roughly 12 000, 16 000, 26 500, and 37 500 Da, respectively. As predicted for an increase in mass with increasing nanocrystal size, the peak shifts to higher *m*/*z* values for samples containing larger

(11) (a) Inoue, H.; Ichiroku, N.; Torimoto, T.; Sakata, T.; Mori, H.; Yoneyama, H. *Langmuir* **1994**, *10*, 4517−22. (b) Nanda, J.; Sapra, S.; Sarma, D. D.; Chandrasekharan, N.; Hodes, G. *Chem. Mater.* **2000**, *12*, 1018−1024.
(12) Cumberland, S. L.; Hanif, K. M.; Javier, J.; Khitrov, G. A.; Strouse, G. F.; Woessner, S. M.; Yun, C. S. *Chem. Mater.* **2002**, *14*, 1576−1584.
(13) Khitrov, G. A.; Strouse, G. F. Single source preparation routes to metal sulfide nanomaterials. Manuscript in preparation.

***Table 1.*** Statistics for ZnS Nanomaterial MALDI-MS Characterization

| abs size (nm)[a] | TEM size dispersity[b] | MS *m*/*z* (k amu) | MS fwhm (k amu) | calcd size (nm) (prolate)[c] | calcd size (nm) (sphere) | MS size disperity[d] |
|---|---|---|---|---|---|---|
| 2.5 | | 12.0 | 7.4 | 2.49 (2.99) | 2.64 | 10% |
| 2.9 | | 16.0 | 9.5 | 2.74 (3.29) | 2.91 | 10% |
| 3.5 | | 26.5 | 20.0 | 3.25 (3.90) | 3.45 | 13% |
| 3.7 | 13% | 37.5 | 29.8 | 3.65 (4.37) | 3.87 | 13% |

[a] Size estimated from the position of the absorbance exciton by comparison to previously reported TEM measurements. [b] Measured from TEM measurements in this work. [c] Calculated from MS peak *m*/*z* using the appropriate model. [d] Calculated from MS peak fwhm using the spherical model.

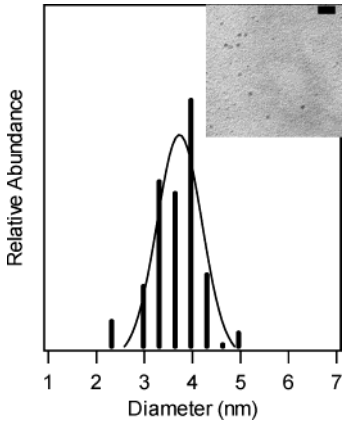


***Figure 2.*** Size distribution obtained from TEM image analysis of 3.7 ± 0.48 nm ZnS-HDA nanocrystals. Curve is a Gaussian function fit to the data. Inset shows one of micrographs used for the measurements (80 kV, 250 000 magnification). Scale bar is 20 nm.

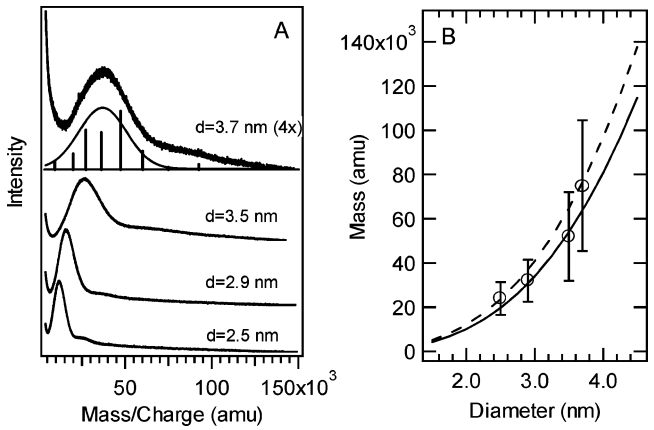


***Figure 3.*** (A) MALDI-MS spectra of 2.5, 2.9, 3.5, and 3.7 nm ZnS-HDA nanocrystals using dithranol as the matrix. The mass distribution for 3.7 nm materials was extrapolated from the size distribution data presented in this figure. (B) Nanocrystal masses projected from MS data assuming +2 species vs masses calculated by assuming spherical (solid line) and prolate (dashed line) nanocrystal morphologies.

nanocrystals. Coupled to the shift, a broadening of the Gaussian peak shape is also observed due to an increase in mass distribution for larger nanocrystals with a fixed size dispersity; that is, a 10 nm diameter ZnS nanocrystal sample will have a mass distribution roughly 8 times larger than a 5 nm sample if both samples exhibit a 10% size distribution. A smaller feature, centered at approximately 2 times the *m*/*z* value of the high-intensity peak, is also observed in the spectra for each nanomaterial. Because of the low signal-to-noise ratio of this feature, values for the center and fwhm of the peak could not be assigned.

To relate the observed mass spectral features to the particle size, the charge (*z*) for the ZnS samples must be known. The charge cannot be directly assigned from the experimental data due to the low resolution of the instrument in the linear mode. However, assuming that the structural motif for the materials is Zn blende and that the nanocrystals exhibit a roughly spherical (or prolate) morphology, the mass and *m*/*z* ratio for the materials can be calculated using eq 1.

$$(\mathrm{ZnS})_n = (\pi/2)N_\mathrm{A}(d^3)/(3V_\mathrm{m}) \qquad (1)$$

The quantity $(\mathrm{ZnS})_n$ in eq 1 is the number of repeating ZnS units in the nanocrystal, $N_\mathrm{A}$ is Avogadro's number, $d$ is the nanocrystal diameter obtained from absorbance or TEM measurements, and $V_\mathrm{m}$ is the molar volume of bulk ZnS. A value of $2.38 \times 10^{22}$ nm$^3$/mol was used for $V_\mathrm{m}$ and was calculated from the density of bulk ZnS having the Zn blende crystal structure.[14] To calculate the mass of a prolate nanocrystal, the $d^3$ term was multiplied by 1.2 to correct for the elongated axis in a prolate nanocrystal, which represents the maximum nanocrystal diameter ratio observed in the TEM studies of the 3.7 nm nanomaterial sample. Comparison of the calculated mass with the *m*/*z* value of the mass spectral feature allows the charges to be assigned.

Comparison of the MS data and calculated masses in Table 1 and Figure 3a indicates that the *m*/*z* position of the peak for each nanomaterial corresponds to roughly one-half the calculated mass of either a spherical or prolate nanocrystal core (Figure 3b) with the organic passivating ligands removed. The relatively small mass difference between spherical and prolate materials and the difficulty in assigning exact morphology in the TEM do not allow the structural motif to be unequivocally assigned. The most probable assignment of this peak is, therefore, a doubly charged nanocrystal species with a nearly spherical motif and most or all passivating ligands removed. Surprisingly, the MS results produce sizes that correlate closely to the values estimated from the position of the absorbance exciton (Table 1) and are within the size distribution limits measured by TEM. This is further verified by direct comparison of the calculated mass distribution for a spherical, 3.7 nm diameter particle to the experimental mass measured by the MALDI-TOF technique (Figure 3a). The lower intensity feature at roughly 2 times the *m*/*z* value of the intense peak could arise from small amounts of singly charged nanocrystals or nanocrystal aggregates. Such aggregates were previously observed in LDI studies of Au nanocrystals.[10a]

The observation of doubly charged ions is not surprising; multiply charged ions are often observed in MALDI-MS measurements of high molecular weight polymers.[5a] It is unusual to only observe a double charged species in such a large system.

(14) *CRC Handbook of Chemistry and Physics*, 59th ed.; Weast, R. C., Ed.; CRC Press: Boca Raton, FL, 1979.

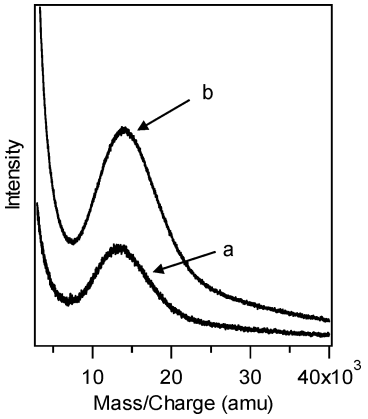


***Figure 4.*** MALDI-MS spectra of 2.5 nm ZnS-HDA nanocrystals using dithranol as the matrix and (a) 50% and (b) 100% laser power.

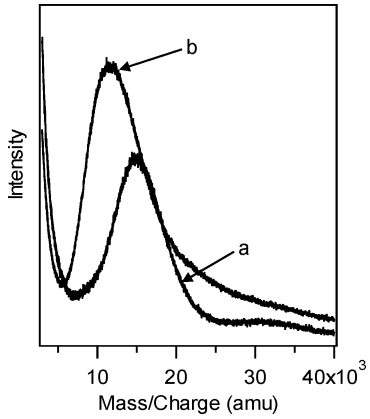


***Figure 5.*** MALDI-MS spectra of 2.5 nm ZnS-HDA nanocrystals using anthracene as matrix and (a) 50% and (b) 100% laser power.

In the mass spectrum of a polymer or biological molecule in the size range of the nanocrystal a significant presence of singly and possibly triply charged species is normally also observed. In fact, in preliminary MALDI-MS studies on CdSe nanomaterials a series of peaks are assignable to singly, doubly, and triply charged nanocrystal species. The apparent anomalous behavior in ZnS may be attributable to the higher ionic character of the ZnS lattice compared to CdSe, which allows the former to consistently retain more charges. It is also possible that the observation of doubly charged ZnS fragments in the MS data may be associated with the lack of direct laser absorption, while the significant absorption cross section of CdSe at 337 nm leads to the production of higher charged species in the MS data. A full understanding of the mechanism of charging in nanocrystalline semiconductors requires further studies, which are underway in our group.

The possibility that the high-intensity MS peak could arise from a singly charged fragment species due to laser-induced ablation was investigated by observing the effects of increased laser power on the spectral features (Figure 4). The lack of a significant change in the peak position or shape suggests that laser ablation does not result in fragmentation of the parent ion. The lack of a *m*/*z* shift further suggests that ZnS nanomaterials are ionized without the ligand shell, which is consistent with the observation of a good correlation between the calculated and measured nanocrystal masses. The capping material is most likely lost in the laser plume, as was previously observed for Au nanocrystal measurements by LDI-TOF MS.[10] Selective ligand ablation is particularly likely for our materials because the hexadecylamine ligand has a finite absorption cross section at 337 nm while the ZnS core does not, and the lattices of ZnS nanocrystals are more ionic in nature, which would tend to weaken the interaction with the passivating layer. This assumption is supported by previously reported ligand exchange dynamics in II−VI nanocrystals.[15]

The effect of changing the matrix on the observed MALDI spectra provides additional evidence for ligand loss from the ZnS nanoparticles. Comparison of the MS data for 2.5 nm ZnS collected in anthracene (Figure 5) shows that the high-intensity peak in anthracene is shifted relative to the dithranol for data collected at 50 and 100% laser power. This shift could be the result of a higher affinity of the less polar anthracene for the hydrophobic tails of the HDA capping groups on the nanocrystals. At the lower laser power more matrix molecules remain associated with the desorbed nanocrystal species, giving rise to a larger *m*/*z* value. At the higher laser power, the closer association of the matrix and ligand results in a more efficient energy transfer, leading to a more efficient removal of ligands from the surface of the nanocrystals and ablating a small amount of core material.

Assignment of the observed *m*/*z* peak as a doubly charged species without a layer of passivating ligands allows the *m*/*z* value, and therefore the size, of the nanomaterial to be discretely assigned (Table 1). The assumption that the average mass arises primarily from unpassivated ZnS materials allows the mass peak line width to be analyzed as a direct measure of the size dispersity of the nanocrystals, as long as isotope contributions and instrumental resolution are included in the calculation. This is achieved by considering the number of ZnS mass units that correspond to a measured mass in the MALDI data, and converting the fwhm for the Gaussian mass profile for each material. For example, in the 3.7 nm ZnS nanocrystals, the size distribution based on TEM imaging is ±13%, or 0.48 nm (Figure 2). This size distribution corresponds to a mass distribution in the 3.7 nm ZnS sample of ±24.5 kDa, or 38%, for a spherical nanocrystal (Table 1). Isotope contributions to the mass increase the fwhm by 0.1% of the observed line width (85 Da for the 3.7 nm ZnS material), and the instrument resolution is expected to contribute another 2% of the *m*/*z* value to the fwhm, or 750 Da. The combined contributions of the above factors predict a ±40% mass distribution on the MALDI experiment for a 3.7 nm ZnS sample, which agrees well with the observed fwhm for the MS peak of ±40 mass %. Further proof of the validity of this approximation can be seen by inspection of the theoretical mass distribution fit of the 3.7 nm MS data shown in Figure 3a, which exhibits a quantitative agreement with the TEM and MS results. Using the same strategy the size distributions for the other samples can be directly calculated for a spherical morphology (Table 1). By inspection of Table 1, the ZnS materials can be systematically correlated with their absolute size and size dispersity and are in full agreement with the optical and TEM results, suggesting that MS could be a powerful tool for rapid sample analysis of II−VI nanomaterials.

Our results show that it is possible to carry out MALDI-MS on inorganic nanomaterials. These studies allow the extrapola-

(15) Murray, C. B.; Norris, D. J.; Bawendi, M. G. *J. Am. Chem. Soc.* **1993**, *115*, 8706.

tion of the MALDI-MS data to the analysis of size measurement and size distributions based on experimentally measured mass data. Both the observed peak position and peak width are consistent with the hexadecylamine-capped ZnS nanocrystal system being studied. Further refinements of this technique such as matrix optimization and variation of fwhm with size distribution as well as applications to other II−VI nanomaterials are currently in progress.

**Acknowledgment.** We wish to thank National Science Foundation CAREER Program (DMR9875940) for financial support of the research. We wish to thank Waters Corporation for the loan of the TofSpec 2E instrument. We also wish to thank Dr. James Pavlovich for helpful assistance and intellectual discussions.

JA035508R